Philosophical Magazine
Publication details, including instructions for authors and subscription information:
http://www.tandfonline.com/loi/tphm20

Failure criterion for metallic glasses

Y. Chen [a], M.Q. Jiang [a], Y.J. Wei [a] & L.H. Dai [a]
[a] State Key Laboratory of Nonlinear Mechanics, Institute of Mechanics, Chinese Academy of Sciences, Beijing 100190, China

Available online: 09 Sep 2011

To cite this article: Y. Chen, M.Q. Jiang, Y.J. Wei & L.H. Dai (2011): Failure criterion for metallic glasses, Philosophical Magazine, 91:36, 4536-4554

To link to this article: http://dx.doi.org/10.1080/14786435.2011.613859

Philosophical Magazine
Vol. 91, No. 36, 21 December 2011, 4536–4554

Taylor & Francis
Taylor & Francis Group

Failure criterion for metallic glasses

Y. Chen, M.Q. Jiang, Y.J. Wei and L.H. Dai*

State Key Laboratory of Nonlinear Mechanics, Institute of Mechanics, Chinese Academy of Sciences, Beijing 100190, China

(*Received 12 January 2011; final version received 8 August 2011*)

Metallic glasses exhibit not only multiple failure modes but also differences in ultimate strength, plastic strain to fracture and asymmetric deviation of failure angles from 45° between tension and compression. The available failure theories cannot fully characterize these phenomena and the underlying physics has not been completely clarified. Here, based on the short-range order structure in metallic glasses, we derive an inherent law that determines when metallic glasses might yield or fracture. A unified failure criterion is constructed which satisfactorily predicts the complex failure behavior observed in metallic glasses. We show that the shear-to-normal strength ratio α and the strength-differential factor β, characterizing shearing resistance between atomic layers and shear-caused dilatation, respectively, have dual control over whether metallic glasses yield in a ductile manner or fracture in brittleness.

Keywords: failure criterion; strength-differential effect; brittle–ductile transition; fracture mechanics; metallic glasses

1. Introduction

Bulk metallic glasses or amorphous alloys are a relatively new class of materials with excellent properties and promising applications [1–4]. The potential applications of metallic glasses (MGs) are closely dependent on their plastic flow and failure behavior [5–13]. Due to the absence of long-range order and dislocation-like defects, plastic deformation at room temperature is prone to be localized into nanoscale shear bands [14–17]. The propagation of single or several dominant shear bands leading to fracture of MGs and the concomitant failure phenomena have attracted the intensive attention of researchers [18–23].

The failure of material starts at the onset of irreversible deformation [24]. It covers the whole process from yielding to final fracture and is usually classified into ductile and brittle failure types. In ductile failure, distinct plastic deformation (yield) is shown before final fracture, while, in brittle failure, fracture ensues immediately after yielding with little plasticity. In crystalline solids, ductile or brittle failure is relatively well understood in terms of movement of dislocations, and it is sufficiently characterized by a single governing parameter, such as the theoretical cleavage-to-shear strength ratio proposed by Kelly et al. [25], or the equivalent

*Corresponding author. Email: lhdai@lnm.imech.ac.cn

ISSN 1478–6435 print/ISSN 1478–6443 online

http://dx.doi.org/10.1080/14786435.2011.613859
http://www.tandfonline.com

parameter representing whether a crack is atomically sharp or blunt by Rice and Thomson [26]. These theories, however, are not suitable for MGs due to their unique atomic structures and resultant failure behaviors, such as failure asymmetry between tension and compression, and multiple fracture modes [27–29].

In MGs, the perplexing failure asymmetry between tension and compression is mainly manifested by three aspects. First, MGs exhibit significant plasticity/ductility difference. The compressive plasticity in MGs has been greatly improved [30–32], but the plasticity in tension is still near-zero at room temperature. This greatly impedes these materials from potential engineering applications. Second, MGs fail along the plane at angle $45^\circ < \theta^T \leq 90^\circ$ under tension and $0^\circ \leq \theta^C \leq 45^\circ$ under compression (Table 1). It is noted that such deviation from 45° is asymmetrical. This implies that the failure of MGs is not solely controlled by the

Table 1. Tensile and compressive failure for different metallic glasses.

	Tensile failure		Compressive failure		
Composites	σ^T (GPa)	θ^T (°)	σ^C (GPa)	θ^C (°)	Ref.
$Pd_{77.5}Cu_6Si_{16.5}$	**1.44**	**50**	**1.51**	**45**	[33]
$Pd_{78}Cu_6Si_{16}$	**1.45**	**55**	**1.54**	**45**	[34]
$Pd_{40}Ni_{40}P_{20}$	**1.46**	**50**	**1.78**	**41.9**	[35]
	1.6	**56**	**1.74**	**42**	[36,37]
$Zr_{40.1}Ti_{12}Ni_{9.3}Cu_{12.2}Be_{26.4}$	**1.98**	**51.6**	**2.0**	**40.8**	[38]
$Zr_{41.2}Ti_{13.8}Ni_{10}Cu_{12.5}Be_{22.5}$	**1.8**	**55**	**2.0**	**44**	[16]
	1.8	**56**	**1.95**	**42**	[39]
	1.89	–	**1.9**	–	[40]
$Zr_{52.5}Ni_{14.6}Al_{10}Cu_{17.9}Ti_5$	**1.65**	**54**	**1.88**	**44**	[41]
	1.66	**60**	**1.82**	**42.5**	[42]
	1.66	**56**	**1.76**	**42**	[43]
$Zr_{55}Al_{10}Cu_{30}Ni_5$	**1.53**	**53**	**1.77**	**41**	[44]
	1.6	–	**1.8**	–	[45]
	1.51	–	**1.82**	–	[46]
$Zr_{56.2}Ti_{13.8}Nb_{5.0}Ni_{5.6}Cu_{6.9}$ -$Be_{12.5}$	**1.487**	**59**	**1.669**	**45**	[47]
$Zr_{57}Cu_{15.4}Ni_{12.6}Al_{10}Nb_5$	**1.2**	–	**1.8**	–	[48]
$Zr_{59}Cu_{20}Al_{10}Ni_8Ti_3$	**1.58**	**54**	**1.69**	**43**	[29]
$Zr_{60}Al_{10}Cu_{20}Pd_{10}$	**1.68**	**55**	**1.88**	**45**	[2]
$Zr_{60}Al_{10}Cu_{25}Ni_5$	**1.63**	–	**1.76**	–	[44]
$Co_{80}Nb_{14}B_6$	**2.88**	–	**3.47**	–	[35]
$Cu_{60}Zr_{30}Ti_{10}$	**2.0**	–	**2.15**	–	[49]
$Cu_{60}Hf_{25}Ti_{15}$	**2.13**	–	**2.16**	–	[49]
$Pd_{80}Si_{20}$	**1.33**	**90**	–	–	[50]
$(Al_{84}Y_9Ni_5Co_2)_{0.95}Sn_5$	–	**90**	–		[51]
$La_{62}Al_{14}(Cu,Ni)_{24}$	**0.55**	**90**	**0.56**	**40–45**	[52]
$Zr_{52.5}Ni_{14.6}Al_{10}Cu_{17.9}Ti_5$	–	**90**	–		[28]
$Zr_{59}Cu_{20}Al_{10}Ni_8Ti_3$	–	**90**	–		[28]
$Zr_{80}Pd_{20}$	–	**90**	–		[53]
$Zr_{55}Al_{10}Ni_5Cu_{30}$			Break or split		[28]
$Ti_{50}Cu_{20}Ni_{23}Sn_7$			Break or split		[28]
$Fe_{65.5}Cr_4Mo_4Ga_4P_{12}C_5B_{5.5}$			Break		[54]

deviatoric stresses. The pressure or normal stress dependence of yielding is an inherent characteristic in MGs [27,55–58]. Third, many experimental investigations have shown that the failure strength of MGs in uniaxial compression (σ^C) is normally greater than that in uniaxial tension (σ^T) (Table 1). This strength-differential (S-D) effect, earlier discovered in a variety of steels with martensitic, bainitic or Widmanstatten ferrite microstructure [59,60], was attributed to non-linear–elastic interactions between dislocations or interstitial solute atoms [61] or permanent volume expansion during plastic deformation [62]. Certainly, the extent of tension–compression asymmetry in MGs shows a broad range, depending on a variety of factors, such as their composition, presence/absence of inclusions and/or other fracture-initiating features. The failure complexity in MGs is also reflected by various fracture modes, e.g. shear failure, normal tensile fracture and split (Table 1).

These complicated failure behaviors mentioned above greatly challenge the classical Tresca or von Mises criteria [63], both of which only predict shear failure. The Mohr–Column (M-C) criterion has been widely used in the study of yielding or fracture behavior of MGs due to its capability of capturing the S-D effect and the normal stress effect on shear failure [28,29,35,64]. A complication is that this criterion would predict a symmetric deviation of fracture angles from 45°, while, in reality, an asymmetric deviation is usually observed in MGs [16,28,29,56].

Therefore, a number of important questions arise from these observations. What is the origin of this failure asymmetry? What are the governing mechanisms of ductile or brittle failure? Could we predict the diverse fracture modes? Zhang and Eckert [65] proposed a unified tensile fracture criterion for MGs in which multiple *tensile* fracture modes and the brittleness or ductility of MGs are characterized by the shear-to-normal fracture strength ratio. Schroers and Johnson [30] suggested that the good ductility of Pt-rich MG is due to its large Poisson ratio. Lewandowski et al. [66] pointed out that the shear to bulk modulus ratio or Poisson ratio is correlated to the plasticity in MGs. Poon et al. [67] further argued that, besides Poisson ratio, another factor called the local shear modulus fluctuation also exerts an influence on the intrinsic plasticity or ductility of MGs. It is also found that the ductile or brittle fracture in MGs can be revealed by the fracture surface morphologies [16,68–74]. The viscous fracture patterns, such as microscale cell, river-like vein pattern or nanoscale dimples, usually occur in ductile fracture [16,68–72], and they are attributed to the fluid meniscus instability or local softening [16,68,75]. In contrast, brittle fracture is reflected by relative smooth fractograph with nanoscale corrugations or featureless mirror zones, suggesting a local cleavage mechanism [16,73,74,76]. These pioneering works mentioned above provide important basics for us to describe in a unified and quantitative fashion the whole failure process, including plastic deformation and resultant fracture of MGs, which has not been satisfactorily discussed as yet. Meanwhile, significant insights on the atomic structure of MGs have been greatly developed in the last couple of years [77–85], which enables us to build a bridge between the macro-failure behaviors and atomic structures.

In this paper, we carry out an atomic interaction analysis based on the nature of short-range order in MGs. Then, a failure criterion is naturally built involving two critical factors: the shear-to-normal strength ratio α and the strength-differential (S-D) factor β. This criterion not only unifies the failure phenomena observed in

MGs but also reveals unambiguous correlations between the macro-failure and the atomic structure, which provides new insights into the physics underlying failure and plasticity in MGs.

2. Failure criterion for MGs

The deformation of material can be resolved into dilatation and distortion. Failure usually starts from some weak planes due to dilatation-induced normal tension/compression or the shear between the neighboring atomic planes. Weak planes accompanied by localized shear bands or micro-cracks may be caused by atomic bond damage or rupture. Atomic interactions inside materials control the whole failure process, and the cohesive models have built a good bridge between the two [86–90]. At a micromechanical level, plastic deformation in MGs occurs by local shearing of atomic clusters. This shearing is accompanied by inelastic dilatation that produces strain-softening, which results in the formation of intense localized shear bands; fracture typically occurs along a dominant shear band with little plastic flow in tension but appreciable plastic deformation in compression. In this way, we consider an arbitrary atomic layer (radius R_u) inside initial homogeneous MGs (Figure 1); atoms in the upper layer interact with those in the bottom block (radius R_b), with the distance $r = \sqrt{x^2 + z^2}$. A *virtualized* cohesive interface is assumed between the upper layer and the bottom block. Physically, those planes can be failure planes induced by applied stress. Under an external load, the atomic layer has local shearing u or normal displacement v beyond the initial distance, then the distance r changes. It is reasonable to assume that the traction and separation between the upper layer and bottom block obeys a cohesive law. This law describes the whole failure process: with the change of r, the traction across the layer should reach a maximum, then weaken (softening) and eventually vanish, permitting complete decohesion. We next determine the cohesive law, taking into account the fundamental atomic structure and the inter-atomic potential.

In addition to randomness, the intra-cluster packing in MGs shows topological short-range order (SRO) and such an organization beyond the level of individual clusters (first neighbors) gives rise to the medium-range order (MRO) [82]. It was found that the two-body correlation functions become weak and insensitive at a radial

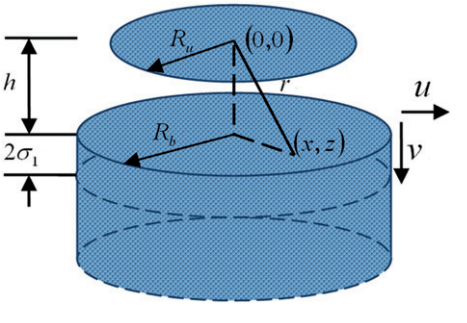

Figure 1. Schematic diagram of a virtualized cohesive interface in MGs.

distance beyond 1 nm [91]. Thus, atomic interactions within MGs should be on a sub-nanometer scale, i.e. in the short-range to the low end of medium-range, as the characteristic scale of the "structure" discussed by Sheng et al. [82]. Being the fundamental building block, SRO greatly influences the physical properties and mechanical response of the glass [92]. This local structure of MGs can be described by the Gaussian radial distribution function (RDF), as suggested by Knuyt et al. [93,94]:

$$RDF(r) = r/(2\pi)^{1/2}(N_1/r_1\sigma_1)\exp[-(r-r_1)^2/2\sigma_1^2]. \tag{1}$$

Here, only the first shell is considered, with a mean position r_1, a width σ_1, and the number of atoms N_1. Atoms are assumed to interact via a Lennard–Jones (L-J) potential that is widely used in molecular dynamics simulation of MGs [27,95,96]:

$$V(r) = 4\varepsilon(\lambda^m/r^m - \lambda^n/r^n) \quad (m > n > 3), \tag{2}$$

where ε is the depth of the potential well, λ the zero-potential distance, and r the distance between two atoms. It should be pointed out that, if more sophisticated atomic potentials are employed, higher-order information and multi-body interactions of atoms [97] might be involved. Actually, the L-J potential captures the major information on atomic interactions and is valid in studying the mechanical behavior of MGs [96]. In particular, the simple form of the L-J potential renders the mathematical derivation tractable.

We next study the interaction between the upper atomic layer and the bottom block separated by a distance h, and first neglect the effect of the upper layer's radius (i.e. $R_u \ll R_b$). The energy due to the atomic interaction is given by $V(r)$ in Equation (2), we then obtain the cohesive energy (i.e. the energy per unit area of the upper atomic layer) for the present model (Figure 1) as:

$$\Phi(h) = 2\pi\rho_u \int_h^\infty \mathrm{d}x \int_0^\infty V(r)RDF(r)/(4\pi r^2)z\mathrm{d}z, \tag{3}$$

where ρ_u is the atomic density of the upper layer, and $RDF(r)$ the atomic distribution in the bottom block. To render the mathematical derivation tractable, we adopt a step function to approximate the atomic density $RDF(r)/(4\pi r^2)$. The density around the first neighbor is set as $\rho_l \approx N_1/8\pi r_1^2\sigma_1$, and the bulk density elsewhere is set as a constant ρ_h. As the cohesive energy is mainly contributed by the atomic interaction in a relatively small r-internal, in particular the overlap region between the radial distribution function and the inter-atomic potential range (e.g. 2–3.5 Å) [93], the integration of Equation (3) can be simply expressed as:

$$\Phi = 4\pi\varepsilon\rho_u\lambda^3\left[\begin{array}{l}\rho_l\left(\dfrac{\lambda^{m-3}}{h^{(m-3)}(m/2-1)(m-3)} - \dfrac{\lambda^{n-3}}{h^{(n-3)}(n/2-1)(n-3)}\right) + (\rho_h - \rho_l) \\ \cdot\left(\dfrac{\lambda^{m-3}}{(r'+\sigma_1)^{(m-3)}(m/2-1)(m-3)} - \dfrac{\lambda^{n-3}}{(r'+\sigma_1)^{(n-3)}(n/2-1)(n-3)}\right)\end{array}\right] \tag{4}$$

where the second term in the square bracket is a correction term with $r' = r_1 \cdot h_1/h_0$ being the upper bound of $h + \sigma_1$, the equilibrium distance $h_0 = \lambda \cdot \sqrt[m-n]{(n-2)/(m-2)}$ and the distance $h_1 = \lambda$ corresponding to the maximum cohesive stress by $\partial\Phi/\partial h = 0$ and $\partial^2\Phi/\partial h^2 = 0$, respectively. Usually, it is convenient to classify the cohesive

energy into the harmonic (symmetric) part and the anharmonic (asymmetric) part; the latter is closely related to the specific properties of amorphous metals [93,94]. In $\Phi(h)$ expressed by Equation (4), these two kinds of energy are totally coupled, thereby we make a satisfactory approximation of $\Phi(h)$ by introducing a simple function $\Psi(h) = C\sin(\frac{\pi(h-h_1)}{2(h_1-h_0)}) + Dv$, where the first term in the right-hand side is harmonic (symmetric, Ψ_s) and the second term is anharmonic (asymmetric, Ψ_a) with the normal deviation $v = h - h_0$. The coefficients C and D stand for the magnitude of harmonic energy and the gradient of anharmonic energy, respectively. They are determined by $\Psi(h_0) = \Phi(h_0)$ and $\Psi(h_1) = \Phi(h_1)$, given by:

$$C = 4\pi\varepsilon\rho_u\rho_l\lambda^3\left[\left(\frac{m-2}{n-2}\right)^{n-3/m-n}\left(\frac{2}{(n-2)(n-3)} - \frac{2}{(n-2)(m-3)}\right) - C_1\right] \tag{5a}$$

$$D = \Phi(h_1) = 4\pi\varepsilon\rho_u\rho_l\lambda^3\left[\left(\frac{2}{(m-2)(m-3)} - \frac{2}{(n-2)(n-3)}\right) + C_1\right]\Big/(\lambda - h_0) \tag{5b}$$

in which

$$C_1 = \left(\frac{\rho_h}{\rho_l} - 1\right)\left(\frac{\lambda^{m-3}}{(r' + \sigma_1)^{(m-3)}(m/2-1)(m-3)} - \frac{\lambda^{n-3}}{(r' + \sigma_1)^{(n-3)}(n/2-1)(n-3)}\right).$$

Now, we impose the bottom block a shear displacement u deviated from the equilibrium position. Equation (4) is independent of u because sliding does not change the interaction for $R_u \ll R_b$. In reality, R_u is not much smaller than R_b, and the influence of shear on the cohesive energy should be considered. Here, we introduce an effective shearing αu, and the new distance is $h = \sqrt{(h_0 + v)^2 + (\alpha u)^2}$, where α measures the shear resistance between two atomic layers. A larger α means a more difficult shear or a stronger internal friction inside the materials. The cohesive normal and shear stresses can thus be calculated by:

$$\sigma = \frac{\partial\psi}{\partial v} = C\cos\left(\frac{\pi(h-h_1)}{2(h_1-h_0)}\right)\frac{\pi}{2(h_1-h_0)}\frac{h_0+v}{h} + D \tag{6a}$$

$$\tau = \frac{\partial\psi}{\partial u} = C\cos\left(\frac{\pi(h-h_1)}{2(h_1-h_0)}\right)\frac{\pi}{2(h_1-h_0)}\frac{\alpha^2 u}{h}. \tag{6b}$$

Interestingly, we find that these two stress components follow the cohesive law as below:

$$(\sigma/\bar{\sigma}_0 + \beta)^2 + (\tau/(\alpha\bar{\sigma}_0))^2 = \cos^2(\pi(h-h_1)/2(h_1-h_0)) \tag{7}$$

in which the two critical parameters $\bar{\sigma}_0$ and β are expressed explicitly as:

$$\bar{\sigma}_0 = C\pi/2(h_1 - h_0) \tag{8}$$

and

$$\beta = -D/\bar{\sigma}_0 \tag{9}$$

The intrinsic length scale $\delta = 2h_1 - h_0$ is associated with debonding. In Equation (7), with increasing surface separation h ($h \leq \delta$), the right-hand term (measuring the extent of cohesion) reaches a maximum when $h = h_1$, then decreases to zero when $h = \delta$, leading to macro-failure. It describes the whole process from elastic deformation to initial softening and then to final fracture. When the applied stresses overcome the effective cohesive strength, the cohesion starts to weaken and failure ensues. Thereby, a failure criterion can be derived as:

$$(\sigma/\bar{\sigma}_0 + \beta)^2 + (\tau/(\alpha\bar{\sigma}_0))^2 = 1. \tag{10}$$

We note that the two terms of the left hand determine whether materials yield in ductile manner or fracture in ideal brittleness. When the first term plays a leading role, a normal-stress dominant failure should occur, suggesting the brittle nature of the materials. Otherwise, shear yielding would lead to ductile failure in materials. As a failure criterion, it should cover the failure characterization ranging from totally ductile to extremely brittle, and unify yielding in the ductile range with fracture in the brittle range [98]. In this criterion, the ductile or brittle behavior actually depends upon the material parameters α and β, which will be discussed in the following sections.

It is noted that criterion (10) involves three factors α, β, and $\bar{\sigma}_0$, and they are correlated with the atomic structure and potential. Geometrically, this failure criterion constructs the eccentric ellipse-like failure envelope in the $\tau - \sigma$ stress space (Figure 2). Therefore, the three factors can be also related to the macro-strengths as follows: $\bar{\sigma}_0 = (\sigma^T_{\max} + \sigma^C_f)/2$, $\alpha = \bar{\tau}_0/\bar{\sigma}_0$ and $\beta = (\sigma^C_f - \sigma^T_{\max})/(\sigma^C_f + \sigma^T_{\max})$, corresponding to the long half axis, ellipticity and the eccentricity ratio of the ellipse, respectively. $\sigma^T_{\max}$ is the theoretical tensile strength and σ^C_f can be regarded as

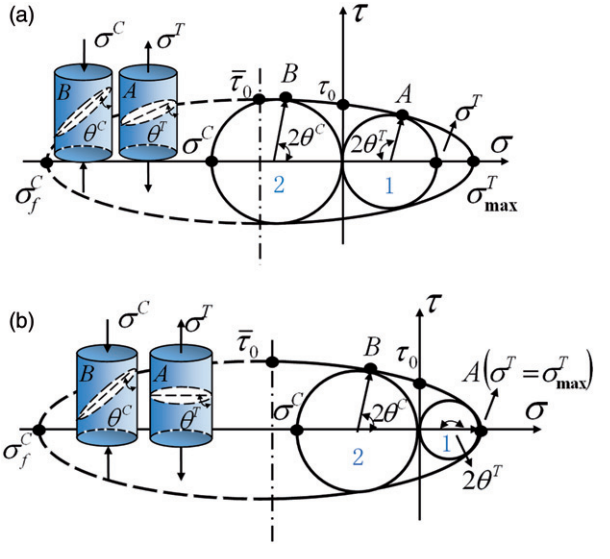

Figure 2. Eccentric ellipse-like failure envelope in the $\tau - \sigma$ stress space: (a) shear failure with $45° < \theta^T < 90°$ and $0° < \theta^C < 45°$; (b) normal tensile fracture with $\theta^T = 90°$.

a fictive theoretical compressive strength, which might be inaccessible in real MGs. As the short half axis, $\bar{\tau}_0$ is the generalized shear strength, which can be reduced to the pure shear strength τ_0 if one ignores the S-D effect. In this case, α is equivalent to the ratio proposed by Kelly et al. [25], or Zhang and Eckert [65]. Physically, the generalized normal strength $\bar{\sigma}_0$ represents the normal resistance to surface failure; the ratio of shear-to-normal strength α reflects the internal friction inside material; and β, which relates to the asymmetrical cohesive behavior, characterizes the tensile/compressive S-D effect and, hence, the dilatant property [62]. The variance of α and β from 0 to 1 can represent not only MGs with minor pressure sensitivity (i.e. $\alpha \to 0$ and $\beta \to 0$) but also those with substantial pressure sensitivity. Since the normal strength $\bar{\sigma}_0$ only controls the overall failure strength and has no effect on failure modes, it will not be involved in following discussions.

3. Unified characterization of failure behavior

In this section, failure criterion (10) presents a unified description of multiple failure behavior in MGs, where the complex failure asymmetry and modes are well covered. Figure 2a and b illustrate failure cases with different shaped ellipses dependent on α and β. These Mohr circles 1 and 2 represent the uniaxial stress states in tension and compression, respectively. Once the Mohr circles contact the failure envelop at tangent points A or B, the material fails with failure angles and strengths marked as θ^T, σ^T or θ^C, σ^C. Figure 2a illustrates the shear failure which produces the failure angles of $45^\circ < \theta^T < 90^\circ$ with respect to the uniaxial tensile axis and $0^\circ < \theta^C < 45^\circ$ with respect to the compressive axis. Failure planes in cylindrical samples in tension (A) and compression (B) are, respectively, displayed as insets, which appear asymmetrical deviations from 45°. A majority of MGs have been observed to fail in this ductile manner (Table 1), and the fracture surface morphology exhibits a characteristic "cell" or "vein" pattern [16,68–72]. Figure 2b, in which the Mohr circle is tangential to the ellipse at its right apex point A, indicating $\theta^T = 90^\circ$ and $\sigma^T = \sigma^T_{\max}$, denotes normal tensile fracture. In some materials, such as La-, and Al-based MGs [51,52], samples follow this ideally brittle mode in tension, where the fracture plane is generally perpendicular to the load axis. On the fractograph, relatively smooth fracture morphology is usually observed with cleavage-like regions [16,74,76]. Split, as an ideally brittle fracture mode, is observed occasionally in special MGs under uniaxial compression [28], in which the failure plane is parallel to the load axis. This will be discussed in more detail latter. Figure 2a,b show that $\sigma^C > \sigma^T$, and also the failure-angle deviation from 45° between tension and compression, is not necessarily symmetric.

To shed light on the underlying mechanisms of failure, a failure map (Figure 3) is constructed from Equation (10). From the map, we find that factors α and β cooperatively control those complicated failure behaviors in MGs. First, the diverse failure modes observed so far are well characterized; second, the transformation threshold from ductile failure to ideally brittle failure is clearly displayed; third, the asymmetrical deviation of failure angles from 45° in tension and compression is quantitatively shown.

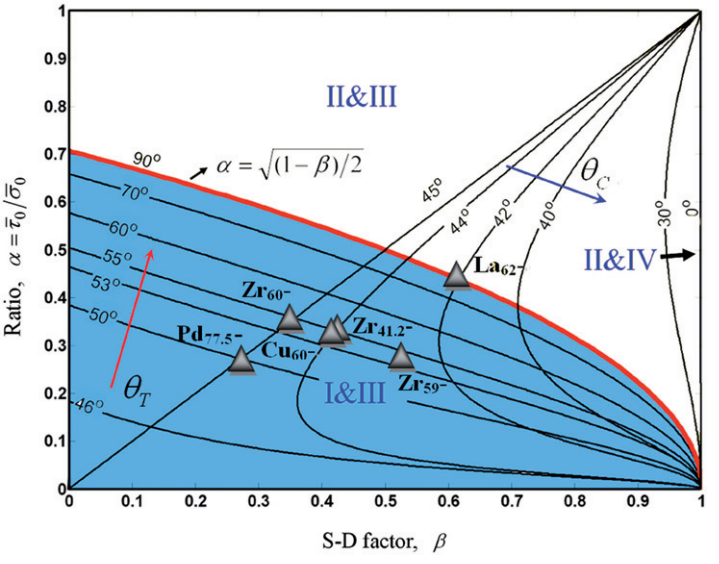

Figure 3. (Color online). Failure map of MGs: dependence of tensile and compressive failure angles on α and β. Typical failure modes, i.e. shear failure (I) and normal tensile fracture (II) in tension, and shear failure (III) and split (IV) in compression, are demonstrated.

In Figure 3, two clusters of isolines of failure angles in uniaxial tension (45°–90°) and compression (45°–0°), respectively, in change with α and β, are presented. The isolines of tensile failure angles range from 45° to 90°, which denotes the process from shear failure to normal tensile fracture. On the other hand, the isolines of compressive failure angles change from 45° to 0°, which shows a gradual transformation from shear failure to split. Accordingly, we can demonstrate four typical failure modes, i.e. shear failure (I) and normal tensile fracture (II) in tension, and shear failure (III) and split (i.e. $\theta^C \to 0°$, IV) in compression. In this way, MGs respectively following I&III (blue region), II&III (white region), and II&IV ($\theta^C \to 0°$) are unified in the map. Note that the red line is the threshold from which fracture occurs along the 90° plane with respect to the load axis. This brittle-ductile transition satisfies:

$$\alpha = \sqrt{(1-\beta)/2} \tag{11}$$

where α and $\sqrt{(1-\beta)/2}$, respectively, represent the resistance of shearing and normal tension between atomic layers, and the competition of the two terms determines the final failure mode. Shearing plays as the dominant failure mode when $\alpha < \sqrt{(1-\beta)/2}$. Otherwise, normal tensile fracture would precede shear yielding, and catastrophic failure occurs. Increasing α means a more difficult activation of shear motion. With an increase in β, $\sqrt{(1-\beta)/2}$ decreases, implying that dilatation promotes normal tensile fracture. Along the transition line, α decreases from $\sqrt{1/2}$ to 0 when β increases from 0 to 1, indicating a higher possibility of ideally brittle fracture. It suggests that tensile ductility not only depend on α but also on β and an increase in any one weakens tensile ductility. Interestingly, if the S-D effect is not

taken into account, i.e. $\beta = 0$, Equation (11) can reduce to the transition condition of tensile fracture mode proposed by Zhang and Eckert [65], i.e. $\tau_0/\sigma^T_{\max} = \sqrt{1/2}$. On the other hand, an ideally brittle fracture in compression, such as split, is found when $\beta \to 1$. Several typical samples of MGs [2,16,29,33,49,52] are marked on the map. Their α values are in the range 0.2–0.5, while β varies from 0.3 to 0.6. We note that ductile MGs, i.e. Zr-, and Pd-based MGs, usually correspond to relative small α and β, while brittle MGs, i.e. La-based MG, usually have large values of α and β. The asymmetrical deviation of angles is also well reflected. Take $Zr_{41.2}Ti_{13.8}Ni_{10}Cu_{12.5}Be_{22.5}$ MG [16], for example; the material fails along the 55° plane in uniaxial tension, but in the 44° plane in compression, which deviate 9° and 1°, respectively, from the maximum shear stress plane. Apparently, both α and β are critical in determining the overall ductility and multiple failure modes of MGs. A smaller α leads to better ductility, either in tension or in compression, due to easier formation of shear bands; a larger β enhances tensile brittleness and ductility difference. Such a failure map may provide useful guidelines to optimize the global ductility in MGs through proper design of α and β.

Since the elastic moduli reflect the inherent strengths of materials, the shear-to-normal strength ratio α virtually represents the competition between shear and normal elastic moduli. A smaller α corresponds to a smaller G/K and a larger v denoting better plasticity. This trend is consistent with previous results [30,66]. The S-D factor β describes the difference in strengths or normal elastic moduli between tension and compression, revealing plasticity asymmetry. For different values of α and β, the unified failure criterion can be classified into several typical cases. If the S-D effect is excluded from our criterion, namely setting $\beta = 0$, the tensile part of the ellipse criterion right reduces to the unified tensile criterion proposed by Zhang and Eckert [65]; specifically, when $\alpha \to 0$, the failure angles $\theta^T \to 45°$ and $\theta^C \to 45°$, which is consistent with the Tresca and von Mises criteria. These criteria are also used to describe the failure behaviors in MGs with minor pressure sensitivity [38,99,100]. If $\beta \neq 0$, when $\alpha \geq \sqrt{(1-\beta)/2}$, normal tensile stress triggers an ideally brittle fracture in MGs and the normal tensile failure will occur along the plane perpendicular to the tensile axis, i.e. $\theta^T = 90°$. This means that the maximum normal stress criterion is one of the special cases for the present criterion. Otherwise, when $0 < \alpha < \sqrt{(1-\beta)/2}$, θ^T will range from 45° to 90° and θ^C will change from 0° to 45°, which agrees well with the M-C criterion.

4. Prediction of failure strength

As an important mode of failure asymmetry, the strength difference between tension and compression is widely observed in soil, concrete, polymers as well as MGs. According to criterion (10), the tensile and compressive failure strength in uniaxial loading can be expressed, respectively, as:

$$\sigma^T/\bar{\sigma}_0 = \begin{cases} 2\left(\alpha\sqrt{(1-\alpha^2)(1-\beta^2)} - \alpha^2\beta\right), & \left(\alpha < \sqrt{(1-\beta)/2}\right) \\ 1-\beta, & \left(\alpha \geq \sqrt{(1-\beta)/2}\right) \end{cases} \tag{12}$$

$$\sigma^C/\bar{\sigma}_0 = \begin{cases} 2\left(\alpha\sqrt{(1-\alpha^2)(1-\beta^2)} + \alpha^2\beta\right), & (\alpha < \sqrt{(1+\beta)/2}) \\ 1+\beta, & (\alpha \geq \sqrt{(1+\beta)/2}). \end{cases} \tag{13}$$

From Equations (12) and (13), we see that the ratio α influences the two failure strengths when $\alpha < \sqrt{(1-\beta)/2}$. However, when $\alpha \geq \sqrt{(1-\beta)/2}$, the effect of α on the tensile strength disappears.

Figure 4 presents the dependence of σ^T and σ^C on α for fixed β, from which general trends can be drawn. Along the black curve ($\beta = 0$), we find that $\sigma^T = \sigma^C$ is always satisfied and that both strengths increase with α until they reach $\bar{\sigma}_0$ at $\alpha = \sqrt{1/2}$. The two clusters of color curves, respectively, show the dependence of σ^T and σ^C on α for $\beta = 0.3,\ 0.4,\ 0.5,\ 0.6$. When $\alpha = 0$, the curves overlap, indicating $\sigma^T = \sigma^C$. When α increases, the difference between the two strengths becomes more significant until it reaches a constant value $2\beta\bar{\sigma}_0$. In fact, we note that, in crystalline metals, pressure or normal stress exerts little effect on the whole failure, namely $\alpha \to 0$. In this situation, shear is prior, both in compression and in tension, and the effect of β is restrained. However, when α is large enough, for example in MGs, the normal stress plays a non-neglected role in the failure process; thus, the influence of β becomes prominent. The same result is also clear from Figure 3, where both of θ^T and θ^C change more quickly with β when α increases. This explains why a single governing parameter is sufficient for crystalline metals but not for MGs. Furthermore, one expects that tension/compression asymmetry ($\beta \neq 0$) is broadly inherent, whether in crystalline metals or in MGs. The ignorable tension/compression asymmetry in crystalline metals may be attributed to their small α (i.e. the shear strength is far smaller than the cleavage strength), which conceals the truth.

Equation (10) indicates that tensile and compressive failure is controlled by both normal stress σ and shear stress τ, but the dependence of shear stress τ on normal

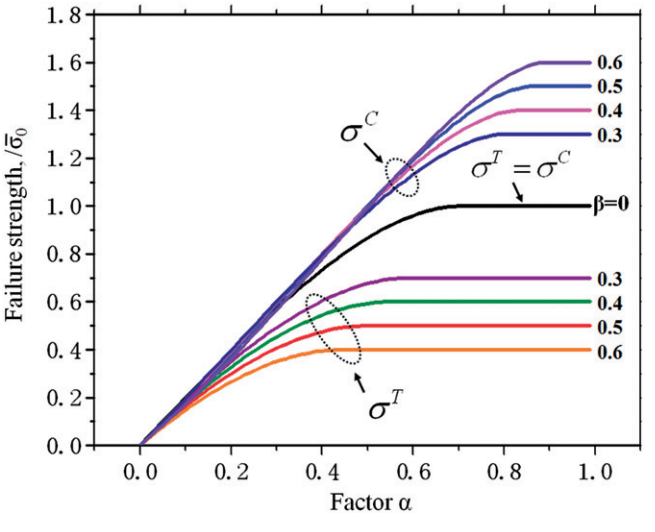

Figure 4. (Color online). Dependence of $\sigma^T$and σ^C on α for fixed $\beta = 0,\ 0.3,\ 0.4,\ 0.5,\ 0.6$.

stress σ is nonlinear. In contrast to the M-C criterion, the unified criterion presents two advantages for the failure prediction of MGs. First, the special failure modes, such as normal tensile fracture and split, which cannot be predicted by the M-C criterion, are well covered in the new one. Second, prediction of the S-D effect from our criterion is better than that from the M-C criterion. Here, we collected data on MGs with all four failure parameters $(\sigma^T, \theta^T, \sigma^C, \theta^C)$ being available (Table 1). The magnitude of the S-D effect is simply deduced from the experimental failure angles of the MGs. For the unified failure criterion, it is given by:

$$\left(\frac{\sigma^C - \sigma^T}{\sigma^C + \sigma^T}\right)_{\text{Unified}} = \frac{\cos(2\theta^C) - \cos(2\theta^T)}{2 - \cos(2\theta^C) - \cos(2\theta^T)} \tag{14}$$

and for the M-C criterion, it is:

$$\left(\frac{\sigma^C - \sigma^T}{\sigma^C + \sigma^T}\right)_{\text{M-C}} = \sin\left(2\theta^T - \frac{\pi}{2}\right). \tag{15}$$

Figure 5 shows the S-D values, respectively, deduced from the unified criterion (10), the M-C criterion and experiments. It was found that the present criterion gives a more reasonable prediction of the S-D effect (8–24%) than the M-C criterion (17–50%), since the experimental result is 1–10%. Considering the inevitable test error and scatter of experimental data, the S-D effect estimated by our criterion is acceptable.

5. Physical mechanisms behind failure

At the microscopic level, we reveal that factors α and β characterize different motions of atomic clusters and thus determine the finial distinct failure behavior in MGs. In an atomic cluster, as illustrated in Figure 6, shear transformation

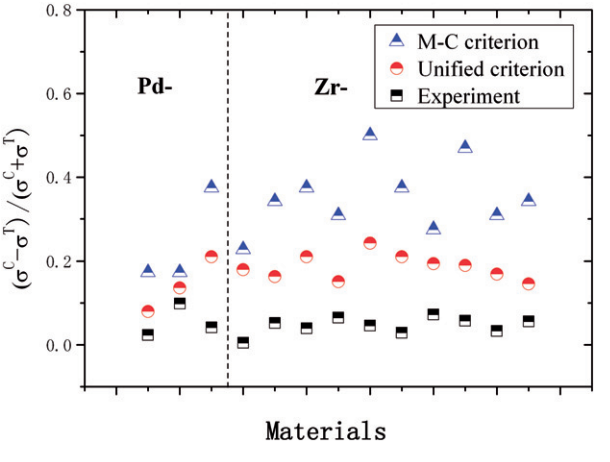

Figure 5. (Color online). Magnitudes of the S-D effect, respectively, predicted by the unified failure criterion and M-C criterion versus experimental results.

is visualized as two rows of atoms around free volume sites, with the atoms in the layers sliding an average atomic distance by overcoming the shear resistance measured by α. This shear operation is activated in atomic clusters when the shear strength is far smaller than normal tensile strength. These shear transformation zones (STZs) induce shear bands to cause shear fracture [5,14,17,101,102], as shown in Figure 2a. During the shear process, the surrounding atoms are pushed apart and new excess free volume is created, which activates tension transformation zones (TTZs) [16,71,72] and leads to shear-caused dilatation (characterized by β). When the atomic bonding is relatively weak, the dilatation-induced tension causes bond rupture in a quasi-cleavage way (Figure 6). Note that this local quasi-cleavage fracture in MGs is not a strictly long-range cleavage and hardly forms a pure cleavage fracture surface as normally found in crystalline materials. Usually, the cleavage-like regions with nanoscale features observed in MGs [73,74,76] are a coupled result of quasi-cleavage and shear due to their shear-dilatancy property [16]. Being independent of direction, the shear operation in STZs contributes to the harmonic cohesive energy Ψ_s, while the other part Ψ_a is due to the asymmetrical behavior of TTZs between tension and compression. A smaller Ψ_s (or α) indicates a lower activation barrier of STZs and, hence, easier shearing. A larger Ψ_a (or β), facilitating the activation of TTZs, corresponds to a stronger dilatation. We find that the magnitudes of α and β are closely dependent on atomic structure and interatomic potential.

The ratio α estimates the difficulty of shear between two atomic layers within materials. In polycrystalline metals, shearing can easily occur along the directions of slip systems, leading to a small α. However, in MGs, due to the lack of long range order, no distinct slip systems exist and the slip between two atomic layers always needs to push surrounding atoms apart, which results in a large α. MGs normally exhibit poorer plasticity than polycrystalline metals, and the plasticity of polycrystalline metals decreases sequentially with the lattice type of their grains: face-centered cubic (fcc), body-centered cubic (bcc) and hexagonal close-packed (hcp) [103]. It confirms that small α facilitates plasticity.

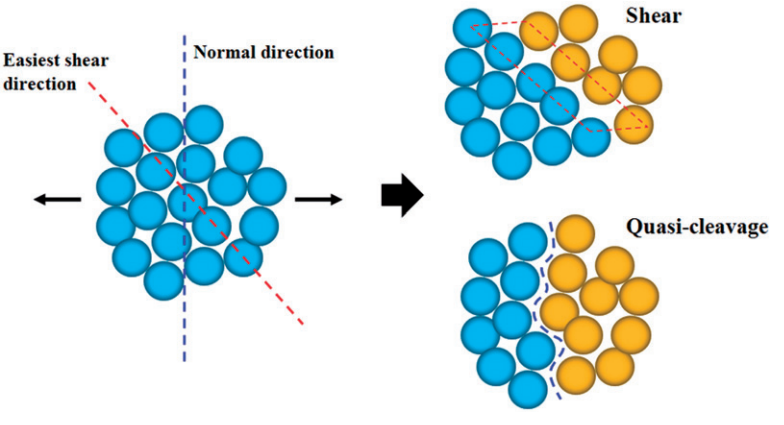

Figure 6. (Color online). Illustration of shear and local quasi-cleavage fracture in atomic scale.

The shear-caused dilatation reflected by β relies on the SRO structure characteristic of atomic packing density ρ_l, mean position r_1, and packing dispersion σ_1. From Equation (9), the dependence of the S-D factor β on the short-range atomic density ρ_l (for a given 6–12 L-J potential and $r_1 = h_0$) and r_1 (for a given 6–12 L-J potential and $\rho_h/\rho_l = 0$) are, respectively, illustrated by Figures 7 and 8. It is obvious that either decreasing ρ_l or increasing r_1 leads to the increase in β in favor of the S-D effect, indicating that the denser short-range atomic packing or smaller deviation of mean atomic position from r_0 corresponds to a weaker S-D effect. Since the atoms residing in the equilibrium position show a balance between

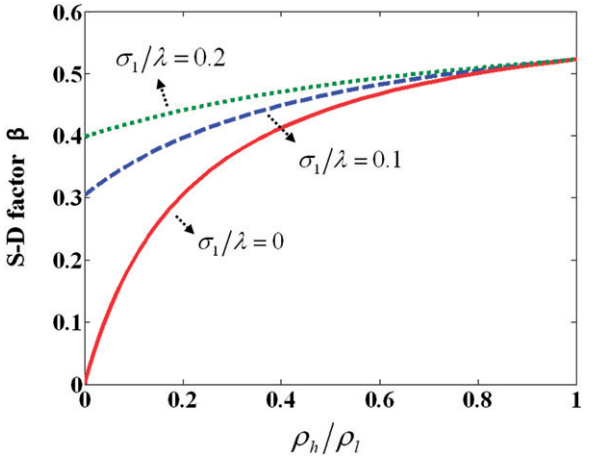

Figure 7. (Color online). Effects of ρ_h/ρ_l on the S-D factor β with fixed $r_1/h_0 = 1$ and the 6–12 L-J potential for $\sigma_1/\lambda = 0$, $\sigma_1/\lambda = 0.1$, and $\sigma_1/\lambda = 0.2$, respectively.

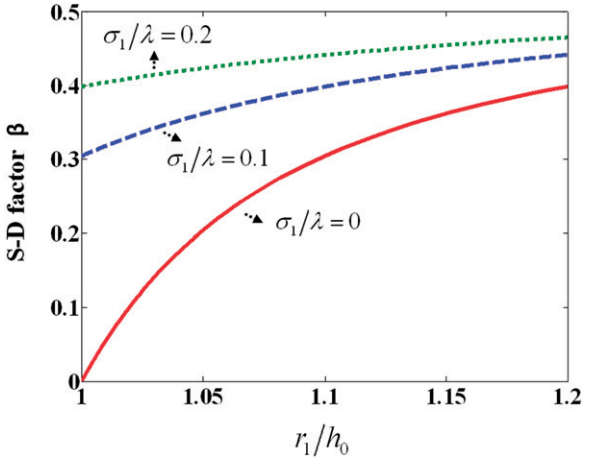

Figure 8. (Color online). Effects of dimensionless mean atomic position r_1/h_0 on the S-D factor β with fixed $\rho_h/\rho_l = 0$ and the 6–12 L-J potential for $\sigma_1/\lambda = 0$, $\sigma_1/\lambda = 0.1$, and $\sigma_1/\lambda = 0.2$, respectively.

tension and compression, the S-D effect should be caused by the atoms distributing far from h_0. We can see that the S-D effect β increases with increasing ρ_h/ρ_l (Figure 7). In the crystalline state, as all nearest neighbor distances in this state tend to be equal to h_0, a minor S-D effect or dilatation is displayed. An extreme case is found when $r_1 = h_0$, $\sigma_1/\lambda \to 0$ and $\rho_h/\rho_l = 0$, in such a perfect ordered structure, the atomic energy should be totally harmonic and the S-D effect should disappear ($\beta \to 0$). Note that the dependence of β on ρ_l and r_1 is significantly weakened when the atomic packing dispersion ($\sigma_1/\lambda = 0,\ 0.1,\ 0.2$) is increasing. This suggests that the atomic packing dispersion plays a critical role in shear dilatation.

Figure 9 illustrates the change in β on the dimensionless atomic dispersion σ_1/λ for the 4–8 (black), 6–12 (red), and 7–14 (blue) L-J potentials when $r_1 = h_0$ and $\rho_h/\rho_l \to 0$. The general trend is that β increases with increasing σ_1/λ. The wider atomic dispersion means a greater topological disorder. It is inferred that more a disordered structure or equivalently, introducing a larger amount of free volume, would enhance the S-D effect in materials and result in better compressive ductility but poorer tensile ductility. In fact, this mechanism has been effectively used to improve the compressive ductility of MGs [30–32]. When $\sigma_1/\lambda \to 0$ (shown by the red mark), $\beta \to 0$, which indicates that the ductility difference vanishes in a perfect ordered structure. As for MGs, σ_1/λ is approximately 0.1 [93,94]; thus, the S-D effect ranges from 0.3 to 0.5 (Figures 7 and 8), which is consistent with the experimentally deduced values (i.e. 0.3–0.6) presented in Figure 3.

It is apparent that a disordered structure renders a relatively larger α and S-D effect than a traditional crystal structure. Usually, STZ operations occur preferentially in MGs, as a relatively small dilatation is required, which leads to shear failure. As an extreme case, when $\alpha \geq \sqrt{(1-\beta)/2}$ in tension, the process of STZs is restrained and that of TTZs is greatly promoted; thus, the material suffers an extreme dilatation but little shearing, resulting in an ideally brittle fracture. It is obvious that the final failure mode results from the competition of STZs and TTZs,

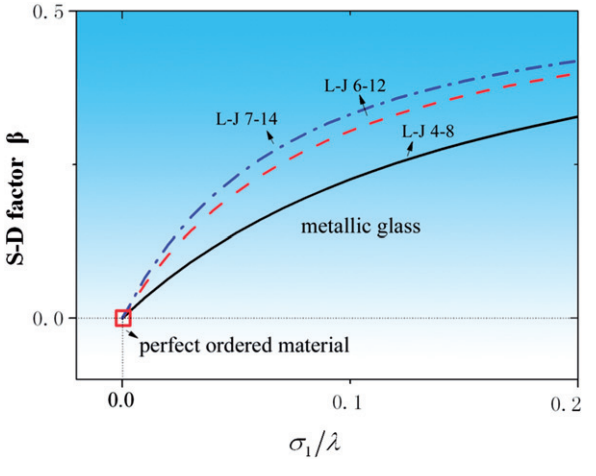

Figure 9. (Color online). Dependence of factor β on the dimensionless atomic dispersion width σ_1/λ with fixed $\rho_h/\rho_l = 0$ and $r_1/h_0 = 1$, respectively, for the 4–8, 6–12, and 7–14 L-J potentials.

which are, respectively, the elementary process of ductile failure [8,75,104,105] and the basis of quasi-cleavage [16,71,72]. Moreover, TTZs arouse pressure sensitivity of plastic flow in MGs [106]. Therefore, the more TTZs that are activated (i.e. larger β), the larger the plasticity difference between tension and compression. This might resolve why in MGs ($\beta > 0$) tensile ductility is normally much poorer than compressive ductility.

6. Conclusions

We propose a unified failure criterion for MGs based on an atomic interaction analysis. Using this new criterion, the observed complex failure phenomena, including multiple failure modes, asymmetrical deviation of failure angles from 45° and the S-D effect between tension and compression, are perfectly characterized. In particular, we find that ductile and brittle failure of MGs is under the dual control of the shear-to-normal strength ratio α and the S-D factor β. Both factors are closely structure-dependent. The disordered structure of MGs results in a relatively large α and β, which implies difficult shearing between atomic layers and significant shear caused dilatation. A single factor, irrespective of α or β, is insufficient to characterize failure behavior of MGs. Tension/compression ductility asymmetry is attributed to factor β, i.e. large β or strong dilatation exerts a negative effect on tensile ductility. The connections between macroscopic failure and the unique atomic structure, as outlined in this paper, should assist in the design of ductile MGs.

Acknowledgements

Financial support from the NSFC (Grants Nos. 10725211, 11002144 and 11021262), the National Natural Science Foundation of China-NSAF (Grant No. 10976100), the National Basic Research of China (Grant No. 2009CB724401), and the Key Project of Chinese Academy of Sciences (Nos. KJCX2-YW-M04) is acknowledged.

References

[1] W.L. Johnson, MRS Bull. 24 (1999) p.42.
[2] A. Inoue, Acta Mater. 48 (2000) p.279.
[3] W.H. Wang, C. Dong and C.H. Shek, Mater. Sci. Eng. R 44 (2004) p.45.
[4] A.L. Greer and E. Ma, MRS Bull. 32 (2007) p.611.
[5] F. Spaepen, Scripta Mater. 54 (2006) p.363.
[6] C. Su and L. Anand, Acta Mater. 54 (2006) p.179.
[7] C. Schuh, T. Hufnagel and U. Ramamurty, Acta Mater. 55 (2007) p.4067.
[8] M.W. Chen, Annu. Rev. Mater. Res. 38 (2008) p.445.
[9] L.H. Dai and Y.L. Bai, Int. J. Impact Eng. 35 (2008) p.704.
[10] M. Martin, L. Meyer, L. Kecskes and N.N. Thadhani, J. Mater. Res. 24 (2009) p.66.
[11] M.M. Trexler and N.N. Thadhani, Prog. Mater. Sci. 55 (2010) p.759.
[12] U. Kuehn, J. Romberg, N. Mattern, H. Wendrock and J. Eckert, J. Mater. Res. 25 (2010) p.368.
[13] W.F. Wu, Y. Li and C.A. Schuh, Phil. Mag. 88 (2008) p.71.
[14] F. Spaepen, Acta Metall. 25 (1977) p.407.

[15] W.H. Jiang, G.J. Fan, F.X. Liu, G. Wang, H. Choo and P.K. Liaw, Int. J. Plasticity 24 (2008) p.1.
[16] M.Q. Jiang, Z. Ling, J.X. Meng and L.H. Dai, Phil. Mag. 88 (2008) p.407.
[17] M.Q. Jiang and L.H. Dai, J. Mech. Phys. Solids 57 (2009) p.1267.
[18] W. Johnson and K. Samwer, Phys. Rev. Lett. 95 (2005) p.195501.
[19] B. Yang, C.T. Liu and T.G. Nieh, Appl. Phys. Lett. 88 (2006) p.221911.
[20] D.L. Henann and L. Anand, Acta Mater. 57 (2009) p.6057.
[21] Z. Han, W.F. Wu, Y. Li, Y.J. Wei and H.J. Gao, Acta Mater. 57 (2009) p.1367.
[22] A. Furukawa and H. Tanaka, Nat. Mater. 8 (2009) p.601.
[23] P. Tandaiya, R. Narasimhan and U. Ramamurty, Acta Mater. 55 (2007) p.6541.
[24] R. Christensen, Mater. Sci. Eng. A 394 (2005) p.417.
[25] A. Kelly, W.R. Tyson and A.H. Cottrell, Phil. Mag. 15 (1967) p.567.
[26] J.R. Rice and R. Thomson, Phil. Mag. 29 (1974) p.73.
[27] C.A. Schuh and A.C. Lund, Nat. Mater. 2 (2003) p.449.
[28] Z.F. Zhang, G. He, J. Eckert and L. Schultz, Phys. Rev. Lett. 91 (2003) p.0455051.
[29] Z.F. Zhang, J. Eckert and L. Schultz, Acta Mater. 51 (2003) p.1167.
[30] J. Schroers and W.L. Johnson, Phys. Rev. Lett. 93 (2004) p.255506.
[31] J. Das, M.B. Tang, K.B. Kim, R. Theissmann, F. Baier, W.H. Wang and J. Eckert, Phys. Rev. Lett. 94 (2005) p.205501.
[32] Y.H. Liu, G. Wang, R.J. Wang, D.Q. Zhao, M.X. Pan and W.H. Wang, Science 315 (2007) p.1385.
[33] L.A. Davis and S. Kavesh, J. Mater. Sci. 10 (1975) p.453.
[34] H. Kimura and T. Masumoto, *Strength, ductility and toughness – a study in model mechanics*, in *Amorphous Metallic Alloys*, F.E. Luborsky, ed., Butterworths, London, 1983.
[35] P.E. Donovan, Acta Metall. 37 (1989) p.445.
[36] T. Mukai, T.G. Nieh, Y. Kawamura, A. Inoue and K. Higashi, Intermetallics 10 (2002) p.1071.
[37] T. Mukai, T.G. Nieh, Y. Kawamura, A. Inoue and K. Higashi, Scripta Mater. 46 (2002) p.43.
[38] J.J. Lewandowski and P. Lowhaphandu, Phil. Mag. A 82 (2002) p.3427.
[39] A.V. Sergueeva, N.A. Mara, J.D. Kuntz, E.J. Lavernia and A.K. Mukherjee, Phil. Mag. 85 (2005) p.2671.
[40] H.A. Bruck, T. Christman, A.J. Rosakis and W.L. Johnson, Scripta Metall. Mater. 30 (1994) p.429.
[41] C.T. Liu, L. Heatherly, D.S. Easton, C.A. Carmicheal, J.H. Schneibel and A. Inoue, Metall. Mater. Trans. A 29 (1998) p.1811.
[42] G. He, J. Lu, Z. Bian, D.J. Chen, G.L. Chen, G.H. Tu and G.J. Chen, Mater. Trans. JIM 42 (2001) p.356.
[43] Z.F. Zhang, J. Eckert and L. Schultz, Metall. Mater. Trans. A 35 (2004) p.3489.
[44] T. Yoshikawa, M. Tokuda and T. Inaba, Int. J. Mech. Sci. 50 (2008) p.888.
[45] V. Keryvin, M.L. Vaillant, T. Rouxel, M. Huger, T. Gloriant and Y. Kawamura, Intermetallics 10 (2002) p.1289.
[46] T. Hirano, H. Matsuo, Y. Kawamura and A. Inoue, Mater. Trans. JIM 41 (2000) p.1454.
[47] F. Szuecs, C.P. Kim and W.L. Johnson, Acta Mater. 49 (2001) p.1507.
[48] R.D. Conner, Y. Li, W.D. Nix and W.L. Johnson, Acta Mater. 52 (2004) p.2429.
[49] A. Inoue, W. Zhang, T. Zhang and K. Kurosaka, Acta Mater. 49 (2001) p.2645.
[50] T. Masumoto and R. Maddin, Acta Metall. 19 (1971) p.725.
[51] A. Inoue, S. Sobu, D.V. Louzguine, H. Kimura and K. Sasamori, J. Mater. Res. 19 (2004) p.1539.
[52] M. Lee, Acta Mater. 52 (2004) p.4121.

[53] J. Saida and A. Inoue, Scripta Mater. 50 (2004) p.1297.
[54] M. Stoica, J. Eckert, S. Roth, Z. Zhang, L. Schultz and W. Wang, Intermetallics 13 (2005) p.764.
[55] K.M. Flores and R.H. Dauskardt, Acta Mater. 49 (2001) p.2527.
[56] R.T. Ott, F. Sansoz, T. Jiao, D. Warner, C. Fan, J.F. Molinari, K.T. Ramesh and T.C. Hufnagel, Metall. Mater. Trans. A 37 (2006) p.3251.
[57] C.H. Hsueh, H. Bei, C.T. Liu, P.F. Becher and E.P. George, Scripta Mater. 59 (2008) p.111.
[58] V. Keryvin, K.E. Prasad, Y. Gueguen, J.C. Sangleboeuf and U. Ramamurty, Phil. Mag. 88 (2008) p.1773.
[59] G.C. Rauch and W.C. Leslie, Metall. Trans. 3 (1972) p.373.
[60] H. Altenbach, G.B. Stoychev and K.N. Tushtev, Int. J. Plasticity 17 (2001) p.719.
[61] J.P. Hirth and M. Cohen, Metall. Trans. 1 (1970) p.3.
[62] D.C. Drucker, Metall. Trans. 4 (1973) p.667.
[63] M.A. Meyers and K.K. Chawla, *Mechanical Behavior of Materials*, Prentice Hall, Upper Saddle River, NJ, 1999.
[64] A. Lund, Acta Mater. 51 (2003) p.5399.
[65] Z.F. Zhang and J. Eckert, Phys. Rev. Lett. 94 (2005) p.094301.
[66] J.J. Lewandowski, W.H. Wang and A.L. Greer, Phil. Mag. Lett. 85 (2005) p.77.
[67] S.J. Poon, A. Zhu and G.J. Shiflet, Appl. Phys. Lett. 92 (2008) p.261902.
[68] X.K. Xi, D.Q. Zhao, M.X. Pan, W.H. Wang, Y. Wu and J.J. Lewandowski, Phys. Rev. Lett. 94 (2005) p.125510.
[69] C. Fan, H. Li, L. Kecskes, K. Tao, H. Choo, P. Liaw and C. Liu, Phys. Rev. Lett. 96 (2006) p.145506.
[70] J.X. Meng, Z. Ling, M.Q. Jiang, H.S. Zhang and L.H. Dai, Appl. Phys. Lett. 92 (2008) p.171909.
[71] R. Raghavan, P. Murali and U. Ramamurty, Acta Mater. 57 (2009) p.3332.
[72] J.P. Escobedo and Y.M. Gupta, J. Appl. Phys. 107 (2010) p.123502.
[73] G. Wang, D.Q. Zhao, H.Y. Bai, M.X. Pan, A.L. Xia, B.S. Han, X.K. Xi, Y. Wu and H.W. Wang, Phys. Rev. Lett. 98 (2007) p.235501.
[74] Z.F. Zhang, F.F. Wu, W. Gao, J. Tan and Z.G. Wang, Appl. Phys. Lett. 89 (2006) p.251917.
[75] A.S. Argon, Acta Metall. 27 (1979) p.47.
[76] M.Q. Jiang, J.X. Meng, J.B. Gao, X.L. Wang, T. Rouxel, V. Keryvin, Z. Ling and L.H. Dai, Intermetallics 18 (2010) p.2468.
[77] D.B. Miracle, T. Egami, K.M. Flores and K.F. Kelton, MRS Bull. 32 (2007) p.629.
[78] T. Egami, J. Metals 62 (2010) p.70.
[79] Y.Q. Cheng and E. Ma, Prog. Mater. Sci. 56 (2011) p.379.
[80] D. Miracle, Acta Mater. 54 (2006) p.4317.
[81] D.B. Miracle, Nat. Mater. 3 (2004) p.697.
[82] H.W. Sheng, Y.Q. Cheng, P.L. Lee, S.D. Shastri and E. Ma, Acta Mater. 56 (2008) p.6264.
[83] H.W. Sheng, W.K. Luo, F.M. Alamgir and J.M. Bai, Nature 439 (2006) p.419.
[84] T. Egami, Prog. Mater. Sci. 56 (2011) p.637.
[85] A.W. Zhu, G.J. Shiflet and S.J. Poon, Acta Mater. 56 (2008) p.593.
[86] G.I. Barenblatt, J. Appl. Math. Mech. 23 (1959) p.1009.
[87] D.S. Dugdale, J. Mech. Phys. Solids 8 (1960) p.100.
[88] A. Needleman, J. Appl. Mech. 54 (1987) p.525.
[89] V. Tvergaard, Mater. Sci. Eng. A 190 (1995) p.215.
[90] L.Y. Jiang, Y. Huang, H. Jiang, G. Ravichandran, H. Gao, K.C. Hwang and B. Liu, J. Mech. Phys. Solids 54 (2006) p.2436.

[91] P.M. Voyles, J.E. Gerbi, M.M.J. Treacy, J.M. Gibson and J.R. Abelson, Phys. Rev. Lett. 86 (2001) p.5514.
[92] E. Pineda, Phys. Rev. B 73 (2006) p.104109.
[93] G. Knuyt, L. de Schepper and L.M. Stals, Phil. Mag. B 61 (1990) p.965.
[94] G. Knuyt and L.M. Stals, Phil. Mag. B 64 (1991) p.299.
[95] Y. Shi and M.L. Falk, Phys. Rev. Lett. 95 (2005) p.095502.
[96] M.L. Falk, Phys. Rev. B 60 (1999) p.7062.
[97] Y.Q. Cheng, E. Ma and H.W. Sheng, Phys. Rev. Lett. 102 (2009) p.245501.
[98] R.M. Christensen, Trans. ASME 73 (2006) p.852.
[99] J. Caris and J.J. Lewandowski, Acta Mater. 58 (2010) p.1026.
[100] R. Varadarajan and J.J. Lewandowski, Metall. Mater. Trans. A 41 (2010) p.1758.
[101] M.A. Meyers, V.F. Nesterenko, J.C. LaSalvia and Q. Xue, Mater. Sci. Eng. A 317 (2001) p.204.
[102] T.C. Hufnagel, Scripta Mater. 54 (2006) p.317.
[103] W.D. Callister Jr, *Fundamentals of Materials Science and Engineering*, 5th ed., Wiley, New York, 2001.
[104] M.L. Falk and J.S. Langer, Phys. Rev. E 57 (1998) p.7192.
[105] D. Pan, A. Inoue, T. Sakurai and M.W. Chen, Proc. Natl. Aced. Sci. USA 105 (2008) p.14769.
[106] L. Sun, M.Q. Jiang and L.H. Dai, Scripta Mater. 63 (2010) p.945.